Plasmonics (2011) 6:337–343
DOI 10.1007/s11468-011-9209-4

Impedance Matching Induce High Transmission and Flat Response Band-Pass Plasmonic Waveguides

Yi Xu · Andrey E. Miroshnichenko · Sheng Lan · Qi Guo · Li-Jun Wu

Received: 13 November 2010 / Accepted: 16 February 2011 / Published online: 25 February 2011

Abstract We consider a model utilizing the concept of impedance matching, which can be applied to design the coupled cascaded plasmonic cavity waveguide with desired properties. We use a transfer matrix method to obtain its transmission and dispersion diagrams. Base on this method, we demonstrate that a band-pass metal–dielectric–metal plasmonic filter with quasi-flat group velocity and tunable bandwidth can be achieved.

Keywords Surface plasmons · Impedance matching · Wavelength filtering

Introduction

It is widely known that electromagnetic waves (EM) suffer from steeper variation at the boundaries with discontinuity of permittivity and permeability, leading to reflection of EMs at the interfaces. The first effort to reduce EM reflection was made by Lord Rayleigh in 1880 [1]. The other great effort to conquer the reflection is the interference-based coatings proposed in 1935 by Alexander Smakula of Carl Zeiss Optics Company. Nowadays, these ideas are generalized and widely used in the EM-related industry.

The concept of impedance matching (IM), in which the input impedance (INI) of an electrical load is designed to match the output one of its corresponding signal source, is firstly proposed to maximize the power transfer from the signal source in electronics. Analog to its electrical counterpart, IM can be applied to other fields where the maximize power output is asked for. The macroscopic transmission lines in microwave [2] as well as the microscopic plasmonic antennas [3, 4], coupled-resonator optical waveguides [5], and the junction of the plasmonic waveguide [6, 7] are the particular examples.

Having the advantage of overcoming the diffraction limit of light, surface plasmon polariton (SPP)-related components can be built in the nanoscale. One of the examples is the SPP channel waveguide which is very important in the high compact optical circuit [8]. A great deal of attention is paid to such kind of waveguide due to its potential application [8–31].

In this paper, we discuss how to use the IM model and transfer matrix method (TMM) to investigate the dispersive coupled cascaded plasmonic cavity waveguide (CCPCW). We show that this model allows one to get a deeper insight of the physical phenomena of bonding and anti-bonding states as well as the SPP Bragg reflector. We would like to mention that a typical physical situation when this model can be employed directly to design a tunable flattop band-pass filter with small group velocity dispersion. The paper is organized as follows. In the section "Model," we describe the theory models about CCPCW. In "Applications of this Model," we give a certain example in which the upper

Y. Xu (✉) · A. E. Miroshnichenko
Nonlinear Physics Centre and Centre for Ultra-high-bandwidth Devices for Optical Systems (CUDOS),
Research School for Physics and Engineering,
Australian National University,
Mills Road (Bldg. 59),
Canberra, ACT 0200, Australia
e-mail: yix124@physics.anu.edu.au

Y. Xu · S. Lan · Q. Guo · L.-J. Wu (✉)
Laboratory of Photonic Information Technology,
School for Information and Optoelectronic Science and Engineering,
South China Normal University,
Guangzhou 510006, People's Republic of China
e-mail: ljwu@scnu.edu.cn

proposed models can work effectively in designing the SPP waveguide components. By comparing with the numerical experiments, the models demonstrate themselves more efficiency to understand the physical properties and obtain the transmission properties of the CCPCW. "Conclusions" concludes the paper.

Model

An infinite plasmonic waveguide, i.e., metal–dielectric–metal (MDM) waveguide can be modeled as a transmission line with a characteristic impedance [6]. Because of its subwavelength width (in our case tens of nanometers), only the symmetric mode is considered. Fabry-Perot (F-P) MDM cavity, a normal plasmonic waveguide component as shown in Fig. 1a, can be modeled as a load connecting to the source by a finite transmission line with characteristic impedance Z_d. Both load and source are regarded as semi-infinite transmission lines with characteristic impedance Z_a in which the subscripts a and d stand for air and dielectric, respectively. By regarding the transverse electric fields as voltage and transverse magnetic fields as a current [6, 16], the characteristic impedance of the two-dimensional infinite transmission line which represents the output impedance can be obtained as:

$$Z_{a,d} \approx \frac{E_x d}{H_y} = \frac{\gamma w}{j\omega\varepsilon_0\varepsilon_{a,d}} \tag{1}$$

where w stands for the width of the MDM waveguide. $\varepsilon_{a,d}$ is the dielectric permittivity of the waveguide core. The INI can be calculated from the lossy transmission line theory [2] as in the following

$$Z_{in} = Z_d \frac{Z_a - iZ_d \tanh(\gamma_d d)}{Z_d - iZ_a \tanh(\gamma_d d)} \tag{2}$$

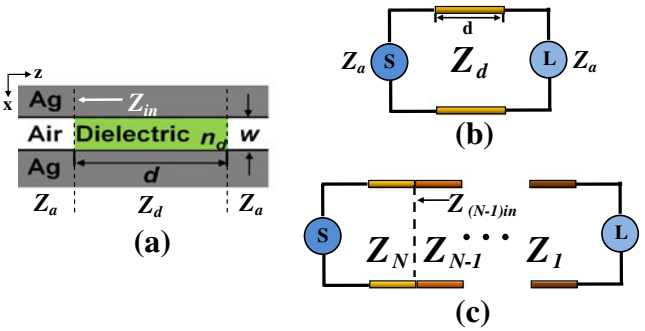

Fig. 1 **a** The structure detail of the F-P MIM waveguide. Z_a and Z_d represent the characteristic impedance of the infinite transmission line when the filling content is air and dielectric (n_d=3.4), respectively. The *white arrow* indicates the effective INI. **b** Electronic analog of the F-P MIM waveguide. **c** Schematic view of N cascaded transmission lines. Z_{N-1} stands for the characteristic impedance of the ($N-1$)th F-P cavity while $Z_{(N-1)in}$ represents the ($N-1$)th INI

where $\gamma_d = \beta_d + j\alpha_d$ represents the complex propagation constant of the fundamental propagating transverse magnetic (the electric field is in the plane of propagation) mode in the MDM waveguide and d stands for the length of the F-P MDM cavity. β determines the guided index. For N transmission lines cascaded between the source and the load as shown by Fig. 1b, we can simplify it as a source with an effective load, and the effective INI can be expressed as

$$Z_{in} = Z_N \frac{Z_{(N-1)in} - iZ_N \tanh(\gamma_N d)}{Z_N - iZ_{(N-1)in} \tanh(\gamma_N d)} \tag{3}$$

where $Z_{(N-1)in}$ can be deduced by the same procedure from the nearest neighbor. With this kind of method, we can describe the INI of any combination of cascaded structures, i.e., CCPCW. The reflection coefficient between the source and effective load can be calculated by

$$R = \frac{Z_{in} - Z_a}{Z_{in} + Z_a} \tag{4}$$

In electronics, people use impedance conjugate matching to maximize the power transferred from the source to the resistive load, i.e., $Z_{out} - Z_{in}^*$ where * denotes the complex conjugate. However, as we can see from Eq. 4, the minimum reflection appears at the condition in which INI is equal to the output impedance. This is the key idea to design band-pass plasmonic waveguide components. The mismatch between the input and output impedance of a waveguide system, $|Z_{in} - Z_{out}|$, gives us an insight into the physical properties of this plasmonic waveguide. In order to obtain the theoretical transmission curve, we use the alternative TMM [32], which is more convenient in obtaining the group velocity and include the dispersive nature of the plasmonic waveguide. Note that we are interested in the deep subwavelength region; the high order modes excited at the impedance discontinuity have a very small decay length compared to the fundamental one. This can be confirmed by looking at the steady state (the pseudovector, magnetic field) obtained by the finite-difference time-domain (FDTD) numerical experiment in which the Drude model [12] is used to obtain the parameters of the metal, and fine grid 1×1 nm is used. From Figs. 2a, we can see that the field pattern at the waveguide discontinues and is dominated by the fundamental mode which means that the reflection from the interface excites mostly the fundamental mode only due to the subwavelength binding. With the pre-find phase shift of the pseudovector at the interface and the assumption of immediately recovering of the fundamental mode these allow one to describe the scattering interface by a simple matrix. It is different from the situation that the waveguide

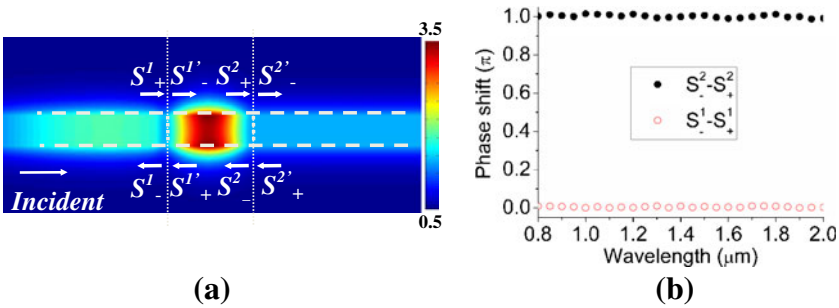

Fig. 2 **a** Steady state (magnetic field) of an impedance discontinuity with left port input. The *dashed lines* outline the structure detail and the *dotted lines* show the referring plane. Incident wavelength is 1.55 μm, w= 0.05 μm, and d=0.17 μm. **b** Phase shifts between $S_-^1\left(S_-^2\right)$ and $S_+^1\left(S_+^2\right)$

junction is wavelength scale, and coefficients of the scattering matrix should be obtained by numerical simulation [7]. Supposing the phase shifts of the reflection are $\phi_{1,2}$, we have $S_-^1 = re^{i\varphi_1}S_+^1, S_-^{1'} = re^{i\varphi_2}S_+^{1'}$ in the left interface. If we choose the referred input and output planes according to the phase shift and suppose the scattering at the interface is elastic and reciprocal, the transfer matrix is well defined. We further look at the reflection phase shift of *Hy* calculated by FDTD, as shown in Fig. 2b, we find that the phase shift of *Hy* when the fundamental mode travel from the metal–air–metal (MAM) to the MDM (or vice versa) is about 0 (π) among the interest spectrum. So the transfer matrix can be written in the manner of Eqs. 5 and 6, which denotes transformation from MAM to MDM and MDM to MAM, respectively.

$$\begin{bmatrix} S_-^1 \\ S_+^1 \end{bmatrix} = \frac{1}{\sqrt{1-r^2}} \begin{bmatrix} 1 & -r \\ -r & 1 \end{bmatrix} \begin{bmatrix} S_+^{1'} \\ S_-^{1'} \end{bmatrix} \tag{5}$$

$$\begin{bmatrix} S_-^2 \\ S_+^2 \end{bmatrix} = \frac{1}{\sqrt{1-r^2}} \begin{bmatrix} 1 & r \\ r & 1 \end{bmatrix} \begin{bmatrix} S_+^{2'} \\ S_-^{2'} \end{bmatrix} \tag{6}$$

where r is the amplitude reflectivity. If we describe the reflection amplitude as $r(\lambda) = \left|\frac{n(\lambda)-1}{n(\lambda)+1}\right|$, $n(\lambda) = \frac{\mathrm{Re}(n_{\mathrm{eff-MAM}}(\lambda))}{\mathrm{Re}(n_{\mathrm{eff-MDM}}(\lambda))}$, the transmission of the F-P cavity can be deduced by the TMM

$$T_s = \left|\frac{1-r^2(\lambda)}{r^2(\lambda)e^{i\delta_d(\lambda)} - e^{-i\delta_d(\lambda)}}\right|^2 \tag{7}$$

Where $r(\lambda)$ and $\delta_{\mathrm{d}}(\lambda) = (\beta_{\mathrm{d}} + j\alpha_{\mathrm{d}})d$ represent reflection amplitude and phase shift accompanied with the loss respectively. γ is obtained by applying the boundary conditions of continuity of the tangential field components [33]. By using the same method as Ref. [34], the group velocity can be derived $V_g(\omega) = DT(\omega)/[y'(\omega)x(\omega) - x'(\omega)y(\omega)]$ where D is the total length of the structure, $x(\omega)$ and $y(\omega)$ are the real and imaginary parts of the complex transmission coefficient, respectively. When calculating the group velocity, the metal loss is not included.

Applications of this Model

It is straightforward to use this model to construct some useful components of an optical circuit. High order filters were theoretically designed and experimentally demonstrated by using microresonators [35–39]. As mentioned above, SPP-related components can manipulate light in a nanoscale. A lot of effort have been paid to construct the first order filter based on the metal–insulator–metal (MIM) waveguide [9, 11, 12, 14–16, 19, 22]. Only several cases paying attention to the subwavelength reflection filter based on higher order bands were considered in the literature [18, 27, 31]. Tao et al. numerically investigate the high order band-pass filter with asymmetrical multiple teeth-shaped structure [23]. A. Pannipitiya et al. proposed a method which is based on the transmission line theory to theoretically describe such a system [25]. Here, using the theory developed above, we propose a high order MDM broadband filter with flattop transmission and quasi-flat group velocity of which is very crucial when the signal is an ultrafast pulse. However, it should be given more attention in the lossy SPP channel waveguide because the matching must be fulfilled both with the real and imagined parts of the impedance.

Having the advantage of flatter passbands, sharper roll-off, and higher out-of-band signal rejection, high order filter becomes an important component of optical integrated circuit.

As have been pointed out by one of the authors, S. Lan, the response of an optical component including large contrast in transmittance as well as the oscillation of group velocity would severely affect the transmission of ultrashort temporal pulses [40].

Lossless total transmission resonance can be modeled with the use of two waveguides coupled directly to an optical cavity. For the simplest transmission resonance model, which can be referred to as the F-P MDM cavity mentioned above, the transmission peak at the output port comes from the constructive multiple interferences at the resonance frequency. From the IM point of view, the INI and the output impedance are both real and is equal to each

other at the resonant wavelength if the system is lossless. As can be seen from Fig. 3a, the EM field at the left end of the F-P is effectively matched at the resonant wavelength. We also notice that the differences between the imaginary parts become more sensitive than the real one when the wavelength moves away from the resonance point. If the metal loss is introduced, the situation is slightly different. From Fig. 3b we can see that the real parts of the input and output impedance match at two points around the red arrows. The imaginary parts, however, match at only one point. We thus name this as quasi-matching since the real and imaginary parts of the impedance cannot match in the same wavelength and the refection still exists. Comparing with the lossless case, quasi-matching changes the transmission slightly (the width of the resonance becomes fat). It is an alternative view to understand why by introducing losses (or the inner loss of the cavity) will enlarge the full high half width of a resonator [13]. Figure 3c gives the transmission results when d is 0.17 μm (black solid line), 2×0.17 μm (black dotted line), and 3×0.17 μm (gray solid line). As one can see that the transmission peaks are corresponding to quasi-match points. Due to more sensitivity in the phase shift, which can be seen from Eq. 2, the resonance is much narrower when the F-P cavity lengths are taken as the high order impedance matching conditions. It means that we can control the spectrum of IM by simply modifying the matching orders. The quasi-matching can only be realized in a narrow spectrum by using a single resonant cavity. It is clear that the transmission is nonflat.

From the above-mentioned analysis, it can be concluded that realizing a flattop broadband filter by utilizing a single

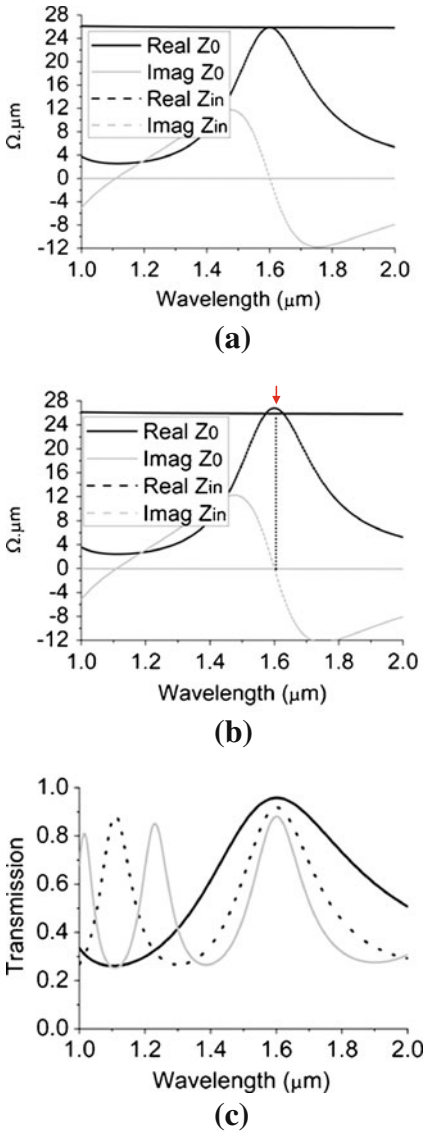

Fig. 3 The real and imagined parts of the input and output impedance of **a** lossless and **b** lossy MIM F-P cavity. **c** Theoretical transmission of the F-P MIM waveguide. The *black solid line* represents the cavity length d=0.17 μm. *Black dotted line* and *gray solid line* stands for $d = 2 \times 0.17\mu$m and $d = 3 \times 0.17\mu$m, respectively

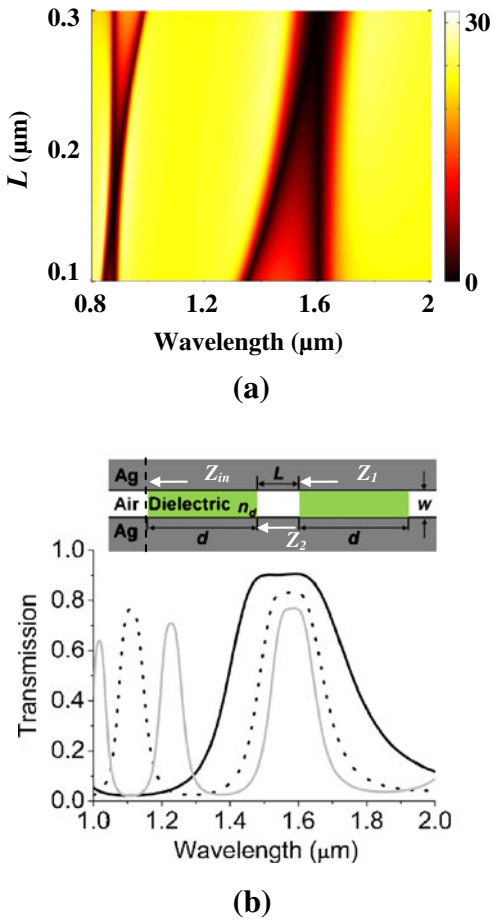

Fig. 4 **a** 2D plot of the input and output impedance mismatch for two F-P cavities. The color scale is corresponding to the value of $|Z_{in} - Z_{out}|$. In the calculation, d=0.17 μm and n_d=3.4. **b** Theoretical transmission of two-coupled F-P MIM waveguide when L=0.22 μm. *Black solid line* represents the cavity length d=0.17 μm. *Black dotted line* and *gray solid line* stands for $d = 2 \times 0.17\mu$m and $d = 3 \times 0.17\mu$m, respectively. *Inset* shows the structure detail

F-P cavity is impossible. To achieve a flat band-pass response with no intensity and group velocity variation over the spectrum, i.e., a broadband IM, it is necessary to use at least two resonators, through which additional parameters can be used to tune the INI. First of all, we consider the case of two coupled identical F-P MDM cavities (d=0.17 μm). Each individual supports a resonance within the bandwidth of interest as shown in the inset of Fig. 4b. Using Eq. 3, the equivalent INI can be derived as:

$$Z_{\text{in}} = \frac{Z_1 Z_a Z_d - iZ_a{}^2 Z_d \tanh(\gamma_a L) - iZ_a Z_d{}^2 \tanh(\gamma_d d) - Z_1 Z_d{}^2 \tanh(\gamma_a L)\tanh(\gamma_d d)}{Z_a Z_d - iZ_1 Z_d \tanh(\gamma_a L) - iZ_1 Z_a \tanh(\gamma_d d) - Z_a{}^2 \tanh(\gamma_a L)\tanh(\gamma_d d)} \tag{8}$$

where Z_1 can be obtain by Eq. 2. The matching map $|Z_{\text{in}} - Z_{\text{out}}|$ for varied coupling lengths among 0.8 to 2 μm is shown by Fig. 4a. By modulating the coupling strength, i.e., the distance L between the two F-P cavities, we can match the real and imaginary parts of the input and output impedance simultaneously. Moreover, when L is larger than 0.22 μm, the impedance can be matched over a band as broad as 130 nm. So the EM fields are effectively continuous at the input plane. It is interesting to note that when L is smaller than 0.15 μm, the analogous bond and anti-bond states [41–43] can also be observed in a very low quality factor system. This kind of phenomenon can be understood as the modulation of the impedance mismatch. The transmission of the coupled F-P cavities can be obtained by cascading the transmission matrixes and have the form

$$T = \left| \frac{(1 - r^2(\lambda))^2}{4r^2(\lambda)\sin^2(\delta_d(\lambda))e^{i(\delta_a(\lambda))} + e^{-i(\delta_a(\lambda))}(r^2(\lambda)e^{i(\delta_d(\lambda))} - e^{-i(\delta_d(\lambda))})^2} \right|^2 \tag{5}$$

Theoretical result of the transmission for L=0.22 μm and d=0.17 μm, 2×0.17 μm, and 3×0.17 μm are presented in Fig. 4b. It can be seen that different matching conditions are corresponding to different bandwidths of flattop

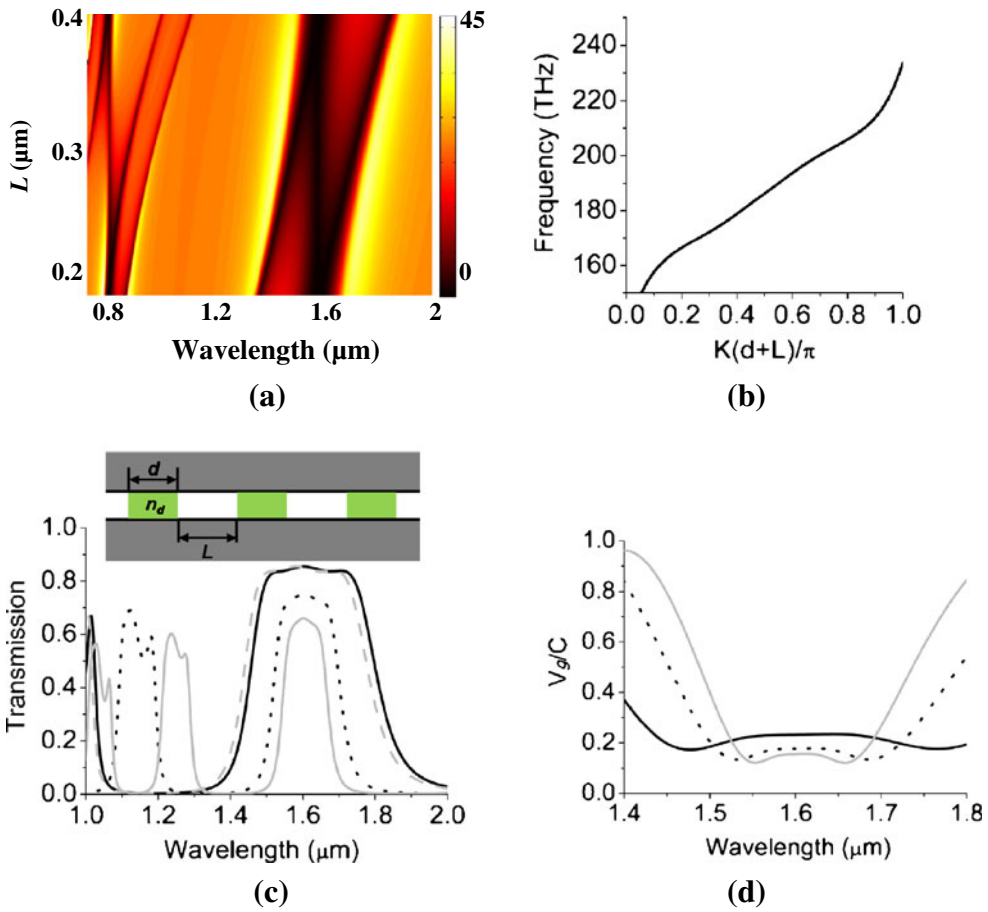

Fig. 5 **a** 2D plot of the input and output impedance mismatch for three F-P cavities. The *color scale* is corresponding to the value of $|Z_{\text{in}} - Z_{\text{out}}|$. In the calculation, d=0.17 μm and n_d=3.4. **b** Dispersion relationship corresponds to a when L is taken to 0.3 μm. **c** Theoretical transmission of the structure shown above the figure (*black solid line* represents the cavity length d=0.17 μm. *Black dotted line* and *gray solid line* stands for $d = 2 \times 0.17\mu$m and $d = 3 \times 0.17\mu$m, respectively), FDTD result (*gray dashed line*). In all the case, L=0.3 μm. **d** The corresponding group velocity

response as mentioned above. High order IM facilitates the narrowing of the passband.

For getting sharper roll-off and higher out-of-band signal rejection, we can cascade more cavities and then modulate the coupling strength by using the same method, i.e., form a CCPCW. For example, we can just add an identical F-P cavity together. It should be noted that we are operating at the passband of the SPP Bragg reflectors. The matching map of $|Z_{in} - Z_{out}|$ is plotted in Fig. 5a. A quasi-flat top passband with a width over 280 nm appears when L= 0.3 μm and d=0.17 μm can be confirmed by Fig. 5a, c. We take the case when d=0.17 μm as an example to validate the theoretical result by the FDTD numerical experiment (shown by the gray dash line). Within this band, the smooth dispersion curve (shown in Fig. 5b) indicates the small variation of the group velocity (shown in Fig. 5d). For comparison, the transmission and the group velocity of the situation $d = 2 \times 0.17\mu$m and $d = 3 \times 0.17\mu$m are plotted in Fig. 5c, d. With more cascaded cavity, the roll-off can be sharper and the out-of-band transmission is further suppressed with the expense of ripple in the transmittance.

Conclusions

It was demonstrated that the proposed IM model provides a general physical picture of the CCPCW while the TMM can describe the transmission properties of the system. We have studied, both analytically and numerically, the box-like band-pass filter by using these methods. The theoretical analysis and FDTD numerical experiment demonstrate that the IM model works well at understanding and designing such component. It allows one to design semi-analytical waveguide components in advances of time consuming simulation. For example, the Bragg reflection filter can be easier understood in terms of IM [9, 11, 16, 19, 22, 27, 28]. A defect mode in the bandgap can be regarded as a perfectly matched state at a certain wavelength. It should be noted that in obtaining the transfer matrix of the scattering interface, we have first numerically calculated the phase shift. If the phase shift is not zero or π, the transfer matrix must be complex, making the whole analysis more cumbersome. We would like to emphasize that this model can also be generalized to a variety of different systems like couple cavities in photonic crystal [43], long period fiber grating [44], etc. In particular, we believe the result of the recent publication [45] can be obtained by modulating the coupling distance between the cavities instead of adding layers at the input and output ports.

Acknowledgments Y. Xu acknowledges the partial support from the China Scholarship Council and the Nonlinear Research Centre at ANU. The work of A.E. Miroshnichenko was supported by the Australian Research Council. L.J. Wu and S. Lan acknowledge the financial support from the National Natural Science Foundation of China (grant nos.10774050 and 10974060) and the Program for Innovative Research Team of the Higher Education in Guangdong (grant no. 06CXTD005).

References

1. Rayleigh L (1880) On reflection of vibrations at the confines of two media between which the transition is gradual. Proc Lond Math Soc 11:51–56
2. Pozar DM (1998) Microwave engineering, 2nd edn. Wiley, NewYork
3. Alù A, Engheta N (2008) Tuning the scattering response of optical nanoantennas with nanocircuit loads. Nat photon 2:307–310
4. Huang JS, Feichtner T, Biagioni P, Hecht B (2009) Impedance matching and emission properties of nanoantennas in an optical nanocircuit. Nano Lett 9(5):1897–1902
5. Ye YH, Ding J, Jeong DY, Khoo IC, Zhang QM (2004) Finite-size effect on one-dimensional coupled-resonator optical waveguides. Phys Rev E 69:056604
6. Veronis G, Fan S (2005) Bends and splitters in metal-dielectric-metal subwavelength plasmonic waveguides. Appl Phys Lett 87:131102
7. Kocabas SE, Veronis G, Miller DAB, Fan S (2008) Transmission line and equivalent circuit models for plasmonic waveguide components. IEEE J Sel Top Quantum Electron 14(6):1462–1472
8. Bozhevolnyi SI, Volkov VS, Devaux E, Laluet JY, Ebbesen TW (2006) Channel plasmon subwavelength waveguide components including interferometers and ring resonators. Nature 440:508–511
9. Wang B, Wang GP (2005) Plasmon Bragg reflectors and nanocavities on flat metallic surfaces. Appl Phys Lett 87:013107
10. Xiao S, Liu L, Qiu M (2006) Resonator channel drop filters in a plasmon-polaritons metal. Opt Express 14:2932–2937
11. Hossieni A, Massoud Y (2006) A low-loss metal–insulator–metal plasmonic bragg reflector. Opt Express 14:11318–11323
12. Han Z, Forsberg E, He S (2007) Surface plasmon Bragg gratings formed in metal-insulator-metal waveguides. IEEE Photonics Technol Lett 19:91–93
13. Yu Z, Veronis G, Fan S, Brongersma ML (2008) Gain-induced switching in metal–dielectric–metal plasmonic waveguides. Appl Phys Lett 92:041117
14. Matsuzaki Y, Okamoto T, Haraguchi M, Fukui M, Nakagaki M (2008) Characteristics of gap plasmon waveguide with stub structures. Opt Express 16:16314–16325
15. Lin XS, Huang XG (2008) Tooth-shaped plasmonic waveguide filters with nanometeric size. Opt Lett 33:2874–2876
16. Hosseini A, Nejati H, Massoud Y (2008) Modeling and design methodology for metal–insulator–metal plasmonic Bragg reflectors. Opt Express 16:1475–1480
17. Gagnon DSLy, Kocabas SE, Miller DAB (2008) Characteristic impedance model for plasmonic metal slot waveguides. J Selected Top Quant Electron 14:1473–1478
18. Park J, Kim H, Lee B (2008) High order plasmonic Bragg reflection in the metal–insulator–metal waveguide Bragg grating. Opt Express 16:413–425
19. Liu JQ, Wang LL, He MD, Huang WQ, Wang DY, Zou BS, Wen SC (2008) A wide bandgap plasmonic Bragg reflector. Opt Express 16:4888–4894
20. Kocabas SE, Veronis G, Miller DAB, Fan S (2009) Modal analysis and coupling in metal–insulator–metal waveguides. Phys Rev B 79:035120

21. Min C, Veronis G (2009) Absorption switches in metal–dielectric–metal plasmonic waveguides. Opt Express 17:10757–10766
22. Gong YK, Wang LR, Hu XH, Li XH, Liu XM (2009) Broad-bandgap and low-sidelobe surface plasmon polariton reflector with Bragg-grating-based MIM waveguide. Opt Express 17:13727–13736
23. Tao J, Huang XG, Lin XS, Zhang Q, Jin XP (2009) A narrow-band subwavelength plasmonic waveguide filter with asymmetrical multiple-teeth-shaped structure. Opt Express 17:13989–13994
24. Zhong ZJ, Xu Y, Lan S, Dai QF, Wu LJ (2010) Sharp and asymmetric transmission response in metal-dielectric-metal plasmonic waveguides containing Kerr nonlinear media. Opt Express 18:79–86
25. Pannipitiya A, Rukhlenko ID, Premaratne M, Hattori HT, Agrawal GP (2010) Improved transmission model for metal-dielectric-metal plasmonic waveguides with stub structure. Opt Express 18:6191–6204
26. Zhang J, Cai LK, Bai WL, Song GF (2010) Flat surface plasmon polariton bands in Bragg grating waveguide for slow light. J Lightwave Technol 28:2030–2036
27. Gong YK, Liu XM, Wang LR (2010) High-channel-count plasmonic filter with the metal–insulator–metal Fibonacci-sequence gratings. Opt Lett 35:285–287
28. Chang YJ, Lo GY (2010) A narrowband metal–multi-insulator–metal waveguide plasmonic Bragg grating. IEEE Photonics Technol Lett 22:634–636
29. Chang YJ (2010) Design and analysis of metal/multi-insulator/metal waveguide plasmonic Bragg grating. Opt Express 18:13258–13270
30. Davoyan AR, Shadrivov IV, Bozhevolnyi SI, Kivshar YS (2010) Backward and forward modes guided by metal–dielectric–metal plasmonic waveguides. J Nanophoton 4:043509
31. Lee PH, Lan YC (2010) Plasmonic waveguide filters based on tunneling and cavity effects. Plasmonics 5:417–422
32. Haus HA (1984) Wave and fields in optoelectronics. Prentice-Hall, Englewood Cliffs
33. Burke JJ, Stegeman GI, Tamir T (1986) Surface-polariton-like waves guided by thin lossy metal films. Phys Rev B 33:5186–5201
34. Bendickson JM, Dowling JP, Scalora M (1996) Analytic expressions for the electromagnetic mode density in finite, one-dimensional, photonic band-gap structures. Phys Rev E 53:4107–4121
35. Little BE, Chu ST, Hryniewicz JV, Absil PP (2000) Filter synthesis for periodically coupled microring resonators. Opt Lett 25:344–346
36. Melloni A (2001) Synthesis of a parallel-coupled ring-resonator filter. Opt Lett 26:917–919
37. Melloni A, Martinelli M (2002) Synthesis of direct-coupled-resonators bandpass filters for WDM systems. J Lightwave Technol 20:296–303
38. Hryniewicz JV, Absil PP, Little BE, Wilson RA, Ho PT (2000) Higher order filter response in coupled microring resonators. IEEE Photonics Technol Lett 12:320–322
39. Little BE, Chu ST, Absil PP, Hryniewicz JV, Johnson FG, Seiferth F, Gill D, Van V, King O, Trakalo M (2004) Very high-order microring resonator filters for WDM applications. IEEE Photonics Technol Lett 16:2263–2265
40. Lan S, Nishikawa S, Ishikawa H (2001) Design of impurity band-based photonic crystal waveguides and delay lines for ultrashort optical pulses. J Appl Phys 90:4321–4327
41. Bayindir M, Temelkuran B, Ozbay E (2000) Tight-binding description of the coupled defect modes in three-dimensional photonic crystals. Phys Rev Lett 84:2140–2143
42. Bayindir M, Ozbay E (2000) Heavy photons at coupled-cavity waveguide band edges in a three-dimensional photonic crystal. Phys Rev B 62:R2247
43. Lan S, Nishikawa S, Sugimoto Y, Ikeda N, Asakawa K, Ishikawa H (2002) Analysis of defect coupling in one- and two-dimensional photonic crystals. Phys Rev B 65:165208
44. Wang ZY, Ramachandran S (2003) Ultrasensitive long-period fiber gratings for broadband modulators and sensors. Opt Lett 28:2458–2460
45. Kang ZW, Lin WH, Wang GP (2009) Dual-channel broadband slow surface plasmon polaritons in metal gap waveguide superlattices. J Opt Soc Am B 26:1944–1948